# THE ELECTRON BACKSCATTERING DETECTOR (eBSD), A NEW TOOL FOR THE PRECISE MUTUAL ALIGNMENT OF THE ELECTRON AND ION BEAMS IN ELECTRON LENSES*

P. Thieberger#, F. Z. Altinbas, C. Carlson, C. Chasman, M. Costanzo, C. Degen, A. Drees, W. Fischer, D. Gassner, X. Gu, K. Hamdi, J. Hock, Y. Luo, A. Marusic, T. Miller, M. Minty, C. Montag, A. Pikin, S. White,
Collider Accelerator Department, Brookhaven National Laboratory, Upton, NY, U.S.A.

*Abstract*

The Relativistic Heavy Ion (RHIC) electron lenses being commissioned to attain higher polarized proton luminosities by partially compensating the beam-beam effect require good alignment of the electron and proton beams. These beams propagating in opposite directions in a 6 T solenoid have an rms width as small as 300 microns and need to overlap each other over an interaction length of about 2 m with relative deviations of less than ~50 microns. A new beam diagnostic tool to achieve and maintain this alignment is based on detecting electrons that are backscattered in close electron-proton encounters. Maximizing the production of these electrons ensures optimum beam overlap. The successful commissioning of these electron backscattering detectors (eBSDs) using 100 GeV/nucleon gold and $^3$He beams is described. Future developments are discussed that could further improve the sensitivity to small angular deviations.

## INTRODUCTION

The partial compensation of the beam-beam effect in RHIC is necessary for mitigating the limit imposed by this effect on the achievable proton-proton beam luminosities. Electron lenses (e-lenses) [1] consisting of low energy (in our case ~6 keV), high intensity (~1 A) magnetized electron beams, can in principle provide the precise non-linear focusing properties necessary to effect such compensations. After developments on a test bench [2], two such e-lenses have now been installed in the RHIC tunnel. In preparation for the 2015 RHIC polarized proton-proton run, commissioning of the RHIC e-lenses has been successfully accomplished [3] with the ion beams available during the 2014 run; namely 100 GeV/nucleon gold and 100 GeV/nucleon helium ($^3$He).

The precise alignment of the electron and ion beams is an important prerequisite for achieving maximum compensation. Over the 2 m interaction region in the ~6 T solenoid, the centers of these ~300 micron rms wide beams need to be separated by less than ~50 microns. The precision achievable with the installed beam position monitoring system [4] isn't quite sufficient for ensuring this result. As described before [5], electron beam electrons backscattered by the relativistic ions or protons (henceforth, ions) can provide the "luminosity" signal required for optimizing and maintaining this alignment.

After briefly reviewing the principle and design of the RHIC electron backscattering detectors (eBSDs), we show results from commissioning the eBSDs with relativistic gold (Au) and helium ($^3$He) beams. We present conclusions about their expected performance with proton beams.

* Work supported by Brookhaven Science Associates under Contract No. DE-AC02-98CH10886 with the U.S. Department of Energy
#pt@bnl.gov

## PRINCIPLE OF THE METHOD

The lensing effect of an e-lens on the relativistic ions is due to the macroscopic electric and magnetic fields produced by the Gaussian-shaped electron beam. In other words, it is the collective long-range Coulomb interaction of the electrons with individual ions that affects the trajectory of these ions. The vast majority of the electron trajectories are only slightly affected since their trajectories are confined by a strong magnetic field. There is however a finite probability for ion-electron collisions with impact parameters that are so small as to produce a significant electron scattering angle imparting at the same time considerable momentum and energy to the scattered electrons. Large scattering angles, correlated with high energies, result in energetic electrons spiraling backwards (towards the electron gun) along the magnetic field lines. As described below, some of these backscattered electrons are intercepted and counted by a scintillation detector placed in air, behind a thin vacuum window.

To first order in the fine structure constant, the Coulomb scattering of relativistic electrons by nuclei is described by the Mott formula which in the rest frame of the nucleus is written as [6]:

$$\frac{d\sigma}{d\Omega} = \frac{Z^2}{4}\left(\frac{e^2}{E}\right)^2 \frac{1}{sin^4\left(\frac{\theta}{2}\right)} \times \left[1 - \left(\frac{pc}{E}\right)^2 sin^2\frac{\theta}{2}\right]$$

$$\times \left[1 + \frac{2E\, sin^2(\theta/2)}{M_A c^2}\right]^{-1} \times \left[1 - \frac{q^2 \tan^2(\theta/2)}{2M_A^2}\right]$$

where σ is the cross section, $Z$ the atomic number , $M_A$ the mass of the nucleus, $e$ the elementary charge, $E$ and $p$ the energy and momentum of the electron in the frame of the nucleus, $\boldsymbol{\theta}$ the electron scattering angle in that frame and $\boldsymbol{q}$ the four momentum transfer coefficient. The first term is the classical Rutherford cross section and the last

ISBN 978-3-95450-141-0

two of the three bracketed corrections (quantum, recoil and magnetic moment respectively) are negligible. Another correction that has been neglected is the one for Bremsstrahlung. A more complete theoretical treatment will probably be required to make good quantitative predictions, especially for even higher energy protons or ions.

Values of this cross section are computed at small angular intervals and then relativistic transformations to the laboratory frame of the cross sections, the angles and the energies lead to results such as plotted in Fig. 1. Such plots are useful for rough estimates of counting rates, but detailed comparisons are difficult due to the complicated nature of the spiraling electron trajectories.

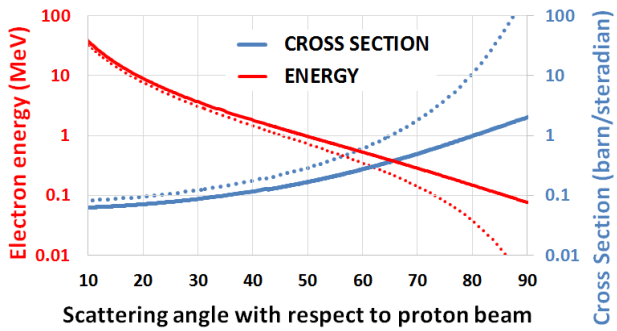


Figure 1: The solid lines show calculated energies and approximate scattering cross sections for 5 keV electrons backscattered by 250 GeV protons. The dotted lines correspond to the same quantities but for 10 eV electrons as a qualitative indication of energetic electrons generated by the interaction of the beam with the residual gas and/or with low energy electrons captured in the potential well of the beam. To obtain quantitative predictions of the effects of the residual gas, the correct treatment of the scattering and ionization of bound electrons will be required and has not yet been performed.

Figure 2 shows the simulated projected trajectories of two electrons backscattered by 250 GeV protons in a 5 T solenoid at angles of $50^0$, one upwards and the other one downwards. As the electrons spiral towards the detector, the radii of their trajectories grow as they encounter lower fields. The upward drift of the trajectory envelopes is due to the horizontal bend in the magnetic field [7].

## IMPLEMENTATION

Each e-lens was equipped with an eBSD consisting of a small plastic scintillator ( 7.4 × 7.9 × 20.6 $mm^3$) attached to a 1.2 m long light guide leading to a small magnetically shielded photomultiplier (PMT) tube (Hamamatsu R3998-02). The signals from this PMT reach the instrumentation rack through a ~90 m long 50 Ω coaxial cable and are amplified and connected to a fast discriminator, the output pulses of which are used to determine the counting rates. The light guide is necessary to keep the PMT far enough from the adjacent magnets so as to enable adequate shielding. This scintillation detector assembly is mounted in air in a vertical shaft at the bottom of which there is a 0.1 mm thick titanium alloy vacuum window facing the scintillator. The vertical position of the detector shaft can be selected so as to locate the bottom of the scintillator at any position from ~1 mm to ~26 mm from the edge of the primary electron beam. This position adjustment can be used as an intensity range selector. An insulated tungsten block (35 × 4.9 × 7.6 $mm^3$) with current detection provides some protection against electron beam heating should the position interlock and limit switch fail. Such a failure actually occurred during commissioning and a vacuum failure was avoided thanks to the tungsten block even though indirect heating was sufficient to melt the scintillator. Since the scintillation detector is in air it was easily replaced.

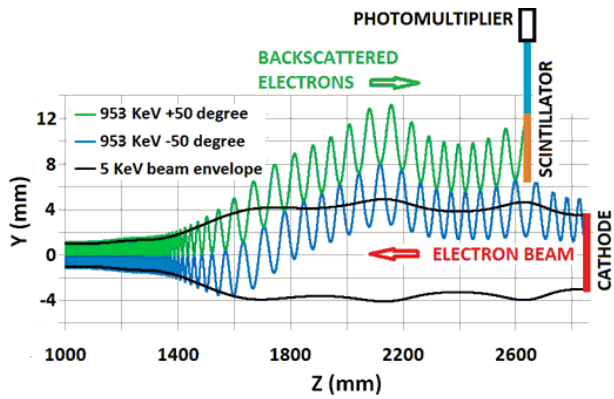


Figure 2: Example of computer simulated electron trajectories starting in a 5 T solenoid field to the left and propagating towards the cathode with some of the trajectories being intercepted by a scintillator (shown schematically). The upward drift of the trajectories is due to the horizontal bend of the magnetic field.

A cutaway drawing of the detector housing is shown in Fig. 3. The backscattered electrons traverse a thin insulated tungsten foil before penetrating the 0.1 mm thick titanium alloy vacuum window and depositing their energy in the plastic scintillator. Current measurement on the thin foil will be used to detect low energy electrons drifting back from the electron collector at the other side of the solenoid.



ISBN 978-3-95450-141-0

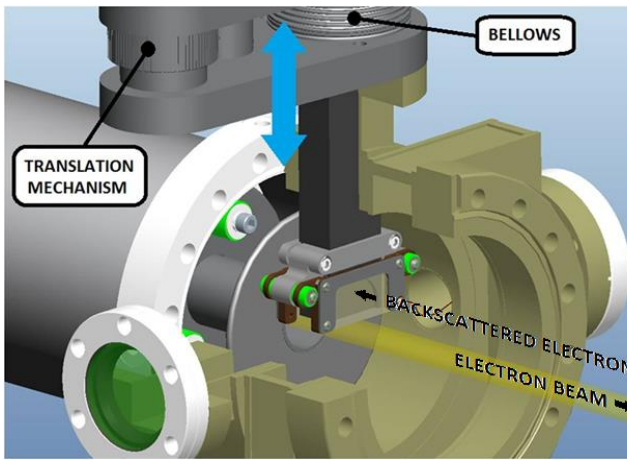


Figure 3: Cutaway drawing of the detector housing, the vertical translation mechanism and a thin tungsten foil located in front of the 0.1 mm thick titanium alloy vacuum window. The area of this window is 25.4 × 6.35 mm$^2$.

## COMMISSIONING WITH GOLD AND He$^3$ BEAMS IN RHIC

The commissioning of the eBSDs was started during the 2014 100 GeV/nucleon gold-gold run. The first proof-of-principle horizontal and vertical beam separation scans are shown in Figs. 4 and 5. The measured widths are the sums in quadrature of the gold and electron beam widths.

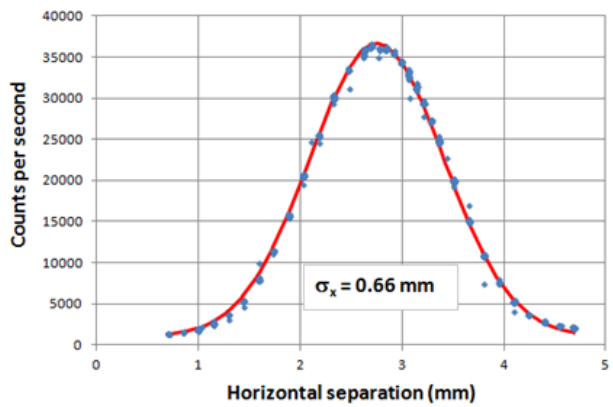


Figure 4: Horizontal beam separation scan obtained by steering the 5 keV electron beam with respect to the 100 GeV/nucleon gold beam.

Soon after obtaining these results, a beam alignment optimization system was implemented based on automatically maximizing both the horizontal and vertical eBSD counting rates. This system is based on a program (LISA) [8] that was developed and used for many years to maximize the luminosities for the RHIC experiments. At the colliding beam interaction points of the high energy physics program, coincidence rates from the zero degree calorimeters (ZDCs) [9] are maximized. Fig. 6 shows the counting rates observed during a manual LISA eBSD scan obtained by displacing the gold beam by means of a set of steering correctors forming a closed orbit bump.

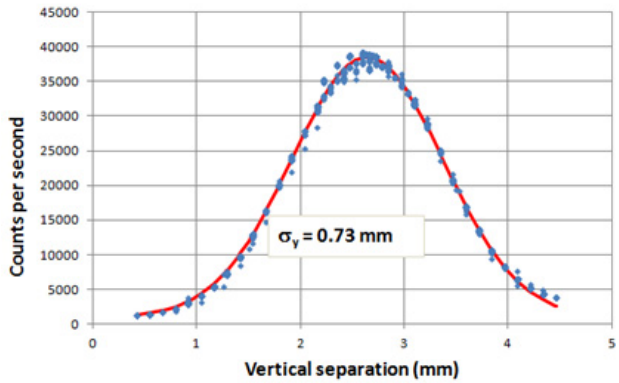


Figure 5: Vertical beam separation scan obtained by steering the 5 keV electron beam with respect to the 100 GeV/nucleon gold beam.

After the gold run was completed, there was a brief opportunity for commissioning the eBSD system with a $^3$He beam. This was important since gold scattering cross sections are much larger than the cross sections for protons. The cross section for $^3$He is only ~4 times larger, and this fact will be compensated by the higher proton beam intensities. In other words, the counting rates observed for $^3$He should be similar to the ones expected for protons.

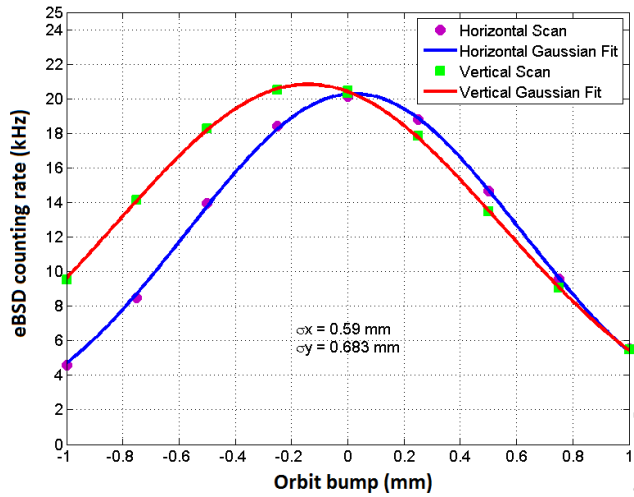


Figure 6: Manual beam separation scans obtained by steering the gold beam with the orbit bumps utilized for the automated alignment optimization system based on the LISA program [8]

During the He$^3$ run the vertical positioning mechanism was utilized for the first time since the counting rates with gold had always been so large that the fully retracted position had to be used. Figure 7 shows the counting rate as function of detector position for a 100GeV/nucleon $^3$He beam consisting of 93 bunches with 4.7E10 ions per bunch and a 6 keV, 88 mA electron beam.

ISBN 978-3-95450-141-0

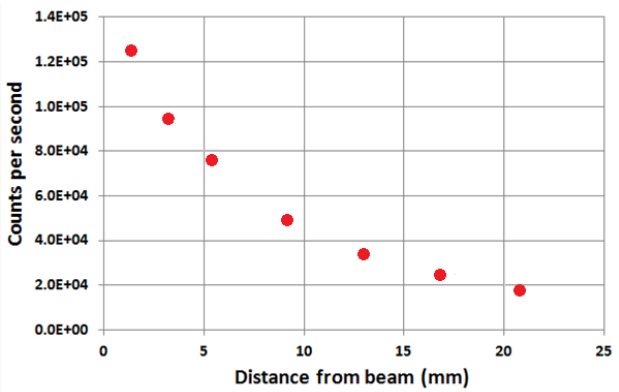


Figure 7: eBSD counting rates as function of detector position. These results were obtained with a 100 GeV/nucleon $^3$He beam consisting of 93 bunches with 4.7E10 ions per bunch and a 6 keV, 88 mA electron beam.

In addition to obtaining total eBSD counting rates, one can also sort and store the counts as function of their time of arrival with respect to a bunch-synchronized clock or with respect to a revolution-synchronized clock. The first choice offers the possibility (at least in principle) of utilizing electron time of flight information to obtain longitudinally dependent luminosities which may be useful for detecting relative angular misalignments between the electron and ion beams. It remains to be seen if this is practical considering bunch lengths and time resolutions.

The second choice provides a very useful display of those bunches that are overlapped by a pulsed electron beam thus allowing convenient and accurate timing adjustments. It also provides display and measurements of back-ground counts due to the interaction of the ion beam with electrons of the residual gas.

During the 2014 run there were brief periods during which some of these ideas could be tested. A fast time digitizer [10] was utilized to obtain the results shown in Fig. 8. The background counts seen in the top plot are due to scattering of atomic electrons belonging to the residual gas. This counting rate is of course very sensitive to the quality of the vacuum. When a pulsed electron beam overlaps the last two bunches preceding the abort gap, the counting rates are ~20 times larger as seen at the bottom of Fig. 8. The small satellite peaks that appear to the left of the larger ones may be due to beam misalignment, but there was no time to investigate this issue further.

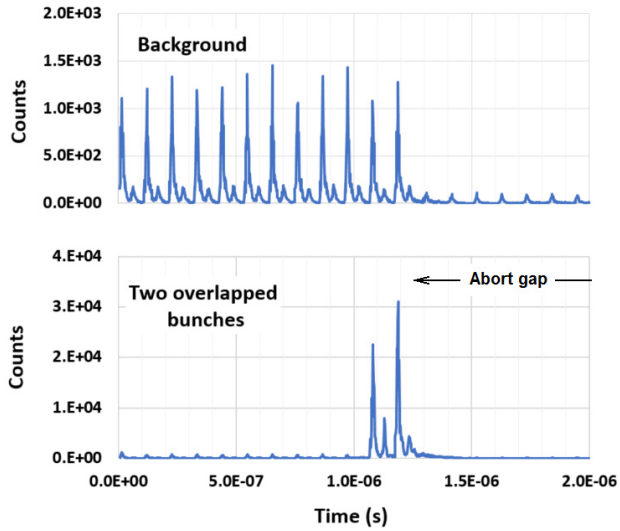


Figure 8: Time distributions with respect to a revolution synchronized clock of eBSD pulses accumulated without (top) and with (bottom) the presence of a 0.15 A pulsed electron beam overlapping the last two bunches. The background pulses are due to scattering of electrons of the residual gas. Note that the vertical scales differ by a factor ~20. The 100 GeV/nucleon gold beam intensity was 1.15 E9 per bunch. Data were accumulated for ~2 minutes for each of the distributions shown.

## CONCLUSIONS

The successful commissioning of the eBSD detectors with gold and He$^3$ beams indicates that it should be possible to achieve the stringent alignment required for the partial compensation of the proton beam-beam effect. Electron time-of-flight spectra similar to the ones shown in Fig. 8 but on a shorter time scale may aid in refining the angular alignment by providing some information regarding longitudinal position dependence of the luminosity contributions. More importantly, angular steering will be simplified in the future by rotating the beams around the centers of the e-lenses instead of a point between them.

The concept of using Coulomb scattered electrons as diagnostic probes for relativistic ion beams will probably find other applications. In particular, the hollow electron lenses suggested for beam halo control in the Large Hadron Collider [11] should be able to benefit from this technique. It could aid in centering the beams (minimizing the counting rate in that case) and in estimating and monitoring the intensity of the halo. Extremely good vacuum will be required to minimize the background counting rate generated by the interaction of the intense central part of the beam with the residual gas.



ISBN 978-3-95450-141-0

## REFERENCES


[1] W. Fischer, *et al.*, IPAC'10, p. 513, (2010), Kyoto, Japan, TUP065.

[2] X. Gu, *et al.*, "The electron lens test bench for the relativistic heavy ion collider at Brookhaven National Laboratory", Nucl. Instr. and Meth. in Phys. Res. A 743, pp. 56-67 (2013).

[3] W. Fischer, *et al.*, "First Experience with Electron Lenses for Beam-Beam Compensation in RHIC", IPAC2014, Dresden, Germany, to be published, and X. Gu *et. al.*, BNL-10090-2013-CP.

[4] D. M. Gassner, *et al.*, Proceedings of DIPAC2011, Hamburg, Germany, MOPD04, page 38.

[5] P. Thieberger, *et al.*, Proceedings of PAC'11, MOP209, p. 489.

[6] F. Halzen and A. Martin, *Quarks and Leptons*, John Wiley and Sons, (1984).

[7] Classical Electrodynamics, J. D. Jackson, John Wiley and Sons, 1962, page 417.

[8] A. Drees and T. D'Ottavio, Proceedings of EPAC 2004, Lucerne, Switzerland, page 911.

[9] C. Adler, *et al.*, "The RHIC Zero Degree Calorimeters", Nucl. Instr. and Meth. in Phys. Res. A 470, pp. 488-499 (2001).

[10] Agilent 53230A, Universal Frequency Counter/Timer, Agilent Technologies.

[11] G. Stancari *et al*., arXiv:1405.2033v3 [physics.acc-ph] and Fermilab Report TM-2572-APC (May 2014).




ISBN 978-3-95450-141-0